Measurement Science and Technology

100 year anniversary
Measurement Science and Technology

PAPER • OPEN ACCESS

Circular-arc array for the pulsed eddy current inspection of thermally insulated pipelines

To cite this article: Ling Yang *et al* 2023 *Meas. Sci. Technol.* **34** 125114

OPEN ACCESS
IOP Publishing
Measurement Science and Technology
Meas. Sci. Technol. **34** (2023) 125114 (9pp)
https://doi.org/10.1088/1361-6501/acf2b2

Circular-arc array for the pulsed eddy current inspection of thermally insulated pipelines

Ling Yang[1], **Jingxin Dang**[2], **Mengfan Yang**[1], **Yixin Dang**[1], **Kai Yuan**[1], **Yan Zhou**[3] **and Bo Dang**[1,*]

[1] Shaanxi Key Laboratory of Measurement and Control Technology for Oil and Gas Wells, Xi'an Shiyou University, Xi'an 710065, People's Republic of China
[2] School of Resources and Environment, University of Electronic Science and Technology of China, Chengdu 611731, People's Republic of China
[3] School of Information Science and Technology, Northwest University, Xi'an 710127, People's Republic of China

E-mail: dangbo@xsyu.edu.cn

Received 22 July 2023
Accepted for publication 22 August 2023
Published 30 August 2023

Abstract
The inspection of corrosion under insulation (CUI) has been identified as a significant challenge in the petroleum and chemical process industries. As some of the most effective strategies, pulsed eddy current (PEC) techniques have proved effective for the measurement of the CUI of pipelines. In this paper, we propose a circular-arc array (CAA) to improve the measurement efficiency for the PEC inspection of thermally insulated pipelines. Based on the PEC system model for inspecting the CUI of pipelines, the magnetic field distribution of the CAA with multiple excitors was investigated. It is shown that the coverage of induced magnetic field gets much larger than that of the single excitor to realize high-efficiency measurements. Moreover, a sparsely distributed receiver array is designed to further improve the signal-to-noise ratio by eliminating the waviness effect due to multiple excitors. Finally, experiments were conducted, and the results demonstrated the effectiveness of the proposed method for the inspection of thermally insulated pipelines.

Keywords: corrosion under insulation, pulsed eddy current, inspection, circular-arc array, thermally insulated pipeline

(Some figures may appear in colour only in the online journal)

1. Introduction

In the petroleum and chemical process industries, the detection of corrosion under insulation (CUI) of pipelines has been extensively investigated with increasing safety concerns. This is because CUI can result in sudden and hazardous leaks, as well as plant shutdowns with a significant decrease in production volumes [1–4]. Several techniques have been developed for detecting various defects in pipelines, such as the visual method [5], radiography [6], ultrasonic guided waves [7, 8], microwaves [9, 10], and eddy current testing [11–14]. Among them, pulsed eddy current (PEC) testing [13, 14], a different form of the eddy current-based technique, is well-known and widely accepted for its noncontact characteristic and potentially large lift-off distance.

Extensive studies on the application of the PEC technique in the CUI inspection of pipelines have been conducted to

* Author to whom any correspondence should be addressed.

improve the inspection performance for metal pipes [15–22]. Fundamental studies of the analytical and numerical solutions of PEC testing of layered structures have been undertaken in [15, 16]. A three-dimensional finite element model of pipeline corrosion defects was established in [17, 18], and the distributions of the current and induced magnetic fields in the pipeline under various defect volumes were simulated. The inner wall flows in the pipe under insulation were detected using the PEC testing method [19], in which a conventional coil probe was used. To enhance the sensitivity of the PEC inspection, a probe consisting of a circular excitation coil and a differential detector was used to inspect the thinning of the pipes' walls through insulation and cladding. The differential detector could avoid the storage of the reference signal before starting the measurements [20]. Additionally, two different sensors, a hall sensor and a search coil sensor, were employed as detectors to confirm the thickness change due to wall thinning in [21]. Another approach involves using a PEC probe consisting of a circular excitation coil and an anisotropic magnetoresistive sensor-embedded differential detector to measure the time-varying magnetic field signals on the axisymmetric excitation coil's axis [22]. Based on the above methods, PEC techniques have been demonstrated to be one of the most effective strategies for the inspection of the CUI of pipelines. However, the effective coverage area is limited in the circumferential direction, and many duplicate measurements are needed for the all-around inspection of the pipe, which may lead to a low inspection efficiency for long-distance oil and gas pipelines.

Considering the requirement of a high inspection efficiency of the CUI of pipelines, the most straightforward approach is to increase the coverage area by using multiple excitors and multiple receiver array. The advances in the eddy current array coil design [23, 24] have improved the inspection speed and promoted accurate depth sizing of cracks, offering additional benefits, such as state-of-the-art imaging, improved surface coverage, and ease of data archiving. For various pipeline-inspection approaches, the use of multiple excitations and receiving sensor arrays has been demonstrated to be effective for improving both the inspection efficiency and resolution [25–28]. For the inspection of thermally insulated pipelines, the magnetic field distribution of the multiple excitations will become complex or even un-homogeneous because of the large lift-off distance of the insulation layer, which may affect the inspection performance [29]. With a pipe-encircling excitation [29], a giant magnetoresistance (GMR) sensor array was employed to detect the CUI. However, pipe-encircling excitation is difficult to implement in practical applications because of the high excitation current.

In this paper, a circular-arc array (CAA) with multiple excitors and sparsely distributed receivers for the high-efficiency PEC inspection of thermally insulated pipelines is presented. Based on the PEC model for inspection of CUI, we proposed a CAA along the circumference direction of the pipeline to realize high-efficiency measurements with a pipeline-inspection crawler and a data-acquisition circuit. Moreover, a sparsely distributed CAA structure was designed to eliminate the effect of waviness distribution of magnetic field due to multiple excitors. The effectiveness of the proposed system was verified by applying it to experiments to inspect metal pipes with different defects.

2. PEC inspection model for thermally insulated pipelines

The structure of the PEC system for the inspection of pipelines with thermal insulation is illustrated in figure 1(a), and the ZOX cross-section is schematically described in figure 1(b). The excitation coil is wound around the magnetic core and positioned outside the pipe. We assumed that the diameter of the pipe is significantly larger than that of the excitation coil. Thus, the coaxial-layered test object can be regarded as a parallel-layered structure, where the excitation coil is normal to the surfaces of each layer with heights of h_1 and h_2 above the first layer from the upper and lower bounds, respectively. Therefore, as shown in figure 1(c), the PEC system model can be simplified into four layers, including cladding, insulation layer, pipeline, and air. Further, the excitation coil's vertical axis is set as the z-axis [22], and the z-axis coordinates of each layer are represented as h_3–h_6. σ_i and μ_i ($i = 1, 2, 3$) are conductivity and relative magnetic permeability of each layer, respectively.

By supplying a pulsed current signal to the excitation coil, as shown in figure 1(d), the eddy current field relating to the electrical and geometry parameters of each layer can be obtained after cutting off the excitation. The effect of thermal insulation can be ignored in the CUI inspection process by considering the large conductivity difference, although the thickness of the thermal insulation layer should be considered in relation to the large lift-off distance. When a corrosion defect occurs in the pipeline, the secondary magnetic field changes with the pipe thickness.

To further investigate the thermally insulated pipeline inspection, we conducted simulations to calculate the magnetic field distribution of the pipelines. In the simulation, the geometrical structure is the same as that in figure 1(c) with metal pipe, thermal insulator and cladding from inner to outer, and the electrical parameters of each layer used in simulation are listed in table 1.

The insulation and the interior of the pipeline were assumed to be nonconductive and nonmagnetic. The number of turns of the excitation coil was set to 600. By supplying a ramp signal with an excitation current of 1 A and a turn-off time of 30 µs, the magnetic field distributions for a standard 6-inch pipe with an insulation layer thickness of 60 mm at sampling times of 5 ms and 10 ms were obtained and are shown in figure 2.

As shown in figure 2, with an early sampling time (after excitation turned-off) of 5 ms, the magnetic field focused on all the excitor, cladding and metal pipe, except the insulations. As a comparison, with a late sampling time of 10 ms, the eddy current diffused and focused mainly on the metal pipe, while the eddy-current field on the cladding is too weak to be observed. Thus, the magnetic field induced by the excitor can reflect the CUI of metal pipes at late sampling time more clearly, even with such a large lift-off distance due to the thickness of the insulation layer. Using this eddy-current property, the CUI

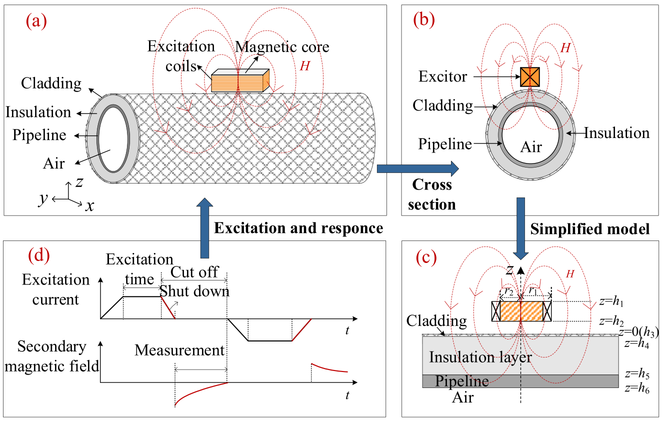

Figure 1. PEC system for a thermally insulated pipeline.

Table 1. Parameters used in simulation.

Test object	Material	Thickness	Electrical parameter
Cladding	Aluminum alloy	0.5 mm	$\sigma_1 = 38$ MS m^{-1}, $\mu_1 = 1$
Insulation	/	60 mm	$\sigma_2 = 0$, $\mu_2 = 1$
Pipeline	Carbon steel	7 mm	$\sigma_3 = 5$ MS m^{-1}, $\mu_3 = 100$

inspection of pipelines can be realized effectively. However, the effective coverage area of such a single excitor is limited in the circumferential direction. Consequently, many duplicate measurements in the circumferential direction are required for the all-around inspection of the pipe, which may lead to a low efficiency for long-distance oil and gas pipelines.

3. CAA for PEC inspection of thermally insulated pipelines

3.1. PEC inspection system for thermally insulated pipelines

To improve the inspection efficiency for practical applications, we investigated the principle of CAA for the PEC inspection of thermally insulated pipelines. The corresponding PEC inspection system with a pipeline-inspection crawler for realizing the motion measurement and a data-acquisition circuit for the CAA is shown in figure 3.

The PEC system for the CUI inspection of thermally insulated pipelines is composed of an automatic pipeline-inspection crawler and a circular-arc PEC array, as shown in figure 3(a). The automatic pipeline-inspection crawler comprises a motor, a gear, a fixed block, a connecting plate, an adjusting rod, and a centralizer wheel, as shown in figure 3(b). The measurement direction was controlled by a motor, and the inspection range of the crawler could be changed by adjusting the rod to meet the inspection requirements of pipelines with different sizes. Figures 3(c) and (d) show the CAA structure (taking five excitors and fifteen receivers as an example) and the corresponding PEC circuits for the CUI inspection of

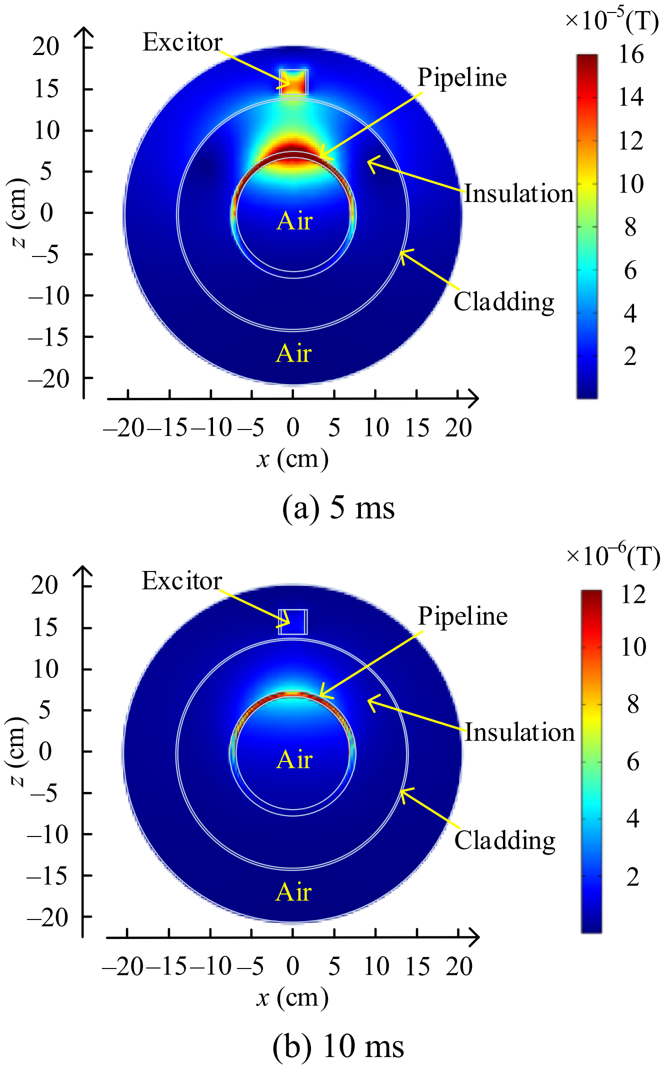

Figure 2. Magnetic field distribution of a single excitor at sampling times of 5 ms and 10 ms.

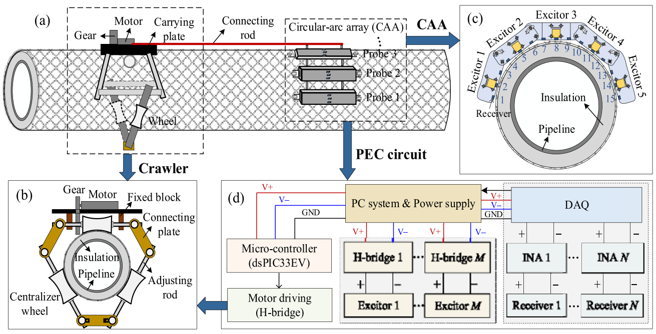

Figure 3. Mechanical structure of the PEC inspection system.

pipelines, respectively, which are designed to realize the excitation, acquisition, and processing of the received CAA signals. In this paper, we use a miniature GMR sensor (AAH002-02) array from the NVE corporation [30] as the receiver. At the excitation end, to avoid mutual electromagnetic interference in the case of individual excitation of each PEC array, the

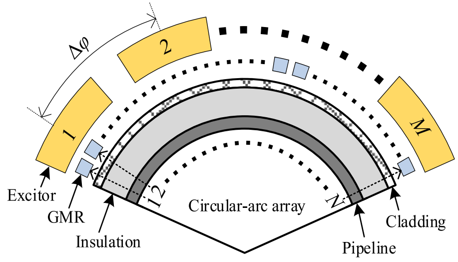

Figure 4. Expansion structure diagram of the circular-arc PEC array with multiple excitors and multiple receivers.

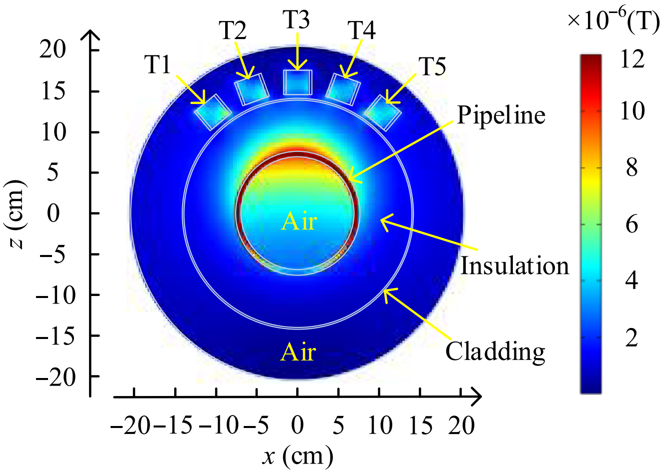

Figure 5. Magnetic field distribution of a circular-arc PEC array at a sampling time of 10 ms.

excitors were excited simultaneously. Note that the inspection of thermally insulated pipelines with different sizes and lift-off distances could be realized by adjusting the spacing of the circular-arc PEC array, as shown in figure 3(c).

3.2. CAA with multiple excitors and multiple receivers

To further investigate the CAA with multiple excitors and multiple receivers, we created a diagram of the CAA structure, which is shown in figure 4.

The circular-arc PEC array comprises M excitors with an azimuth interval of $\Delta\varphi$, and N GMR sensors in the coverage area of the M excitors, which forms a CAA in the circumferential range of the pipe. The number of excitors can be increased or decreased to cover different circumferential ranges of the thermally insulated pipeline. We considered five excitors (termed as T1, T2, T3, T4, and T5) with the element space ($\Delta\varphi$) of 20° as examples. They were uniformly distributed on a circular-arc around the pipe. The azimuths of the excitors were −40°, −20°, 0°, 20°, and 40°, respectively. Figure 5 shows the magnetic field distribution of the circular-arc PEC array for a standard 6-inch pipe with an insulation layer thickness of 60 mm with a sampling time of 10 ms.

Figure 5 shows that the effective coverage area of the magnetic field induced by the circular-arc PEC array increases with the number of excitors. Notably, the coverage of magnetic field is considerably larger than that of the single excitor shown in figure 2(b), even with an insulation layer thickness of 60 mm (the lift-off distances). Using this property, duplicate measurement times in the circumferential direction can be significantly reduced for the all-around inspection of the pipe, and the inspection efficiency can be substantially improved compared to that of the single excitor.

4. Design of sparse CAA

As shown in section 3, the CAA-based PEC system can improve the CUI inspection efficiency of thermally insulated pipelines. However, the distribution of magnetic field may be more inhomogeneous due to the use of multiple excitors. In this Section, we will further optimize the CAA structure to improve the inspection performance. We assumed that the excitation currents for all the excitors are identical. Taking a 6-inch pipe with an insulation layer thickness of 60 mm as an example, the magnetic field in the layer of GMR sensors at sampling time of 10 ms for the three cases, including the single excitor and the CAA with excitor intervals of 20° and 40°, are compared in figure 6.

Figure 6 shows that the coverage area of magnetic field of the excitor array in the circumferential direction of the pipelines is larger than that of the single excitor. Additionally, five peaks correspond to the five excitors, even though the interval of 20° is sufficiently small for neighboring excitors to interact with each other. This is because the observation positions are all outside the insulator with a large lift-off distance. These positions are far from the metal pipes, where the eddy current field appears to be wavy. On the one hand, this waviness effect of the multiple excitors will aggravate the nonuniformity distribution of the magnetic field. On the other hand, the data collected in the sunken area will introduce great errors as well as low SNR because of the too-small value.

Considering the wavy shape of the eddy current field, it would be detrimental to set the GMR sensors at the sunken position of the magnetic field. Moreover, the waviness effect will make the gain of each element of the GMR sensors array quite different, thus complicating the CUI inspection process. As a solution, we chose to set the GMR sensors right under each excitor with respect to the several peaks. This forms a sparsely distributed GMR sensors array that ensures only the magnetic field peaks can be collected and the sunken area is avoided. Taking a CAA with five excitors as an example, the densely, sparsely and uniformly distributed receiving GMR sensors array structures are shown in figure 7.

As shown in figure 7, there exist three kinds of CAA, including the densely, sparsely, and uniformly distributed GMR sensors array. The dense CAA consists of 29 GMR sensors with receiver interval of $\Delta\alpha$ that are densely distributed under the layer of excitors, where the definitions of the excitor interval are the same as those in figure 4. As a comparison, the sparsely distributed GMR array consists of 15 GMR sensors of the total 29 GMR sensors, with index of {2,3,4; 8,9,10; 14,15,16; 20,21,22; 26,27,28}, which can be divided into five groups with respect to five excitors. The receiver interval within each group is still the same as $\Delta\alpha$, and the

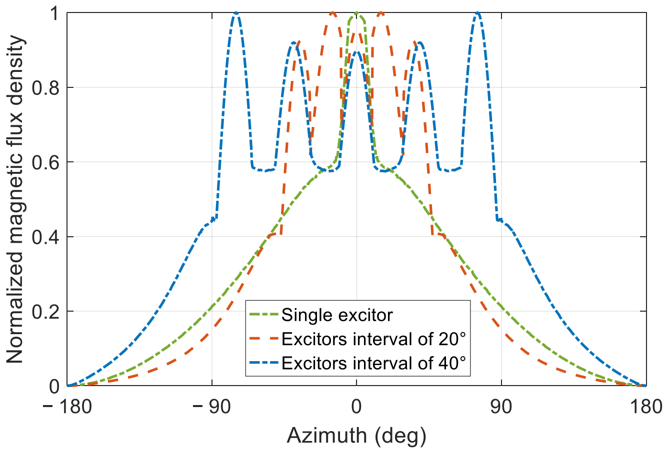

Figure 6. Comparison of the magnetic field distribution produced by different types of excitors.

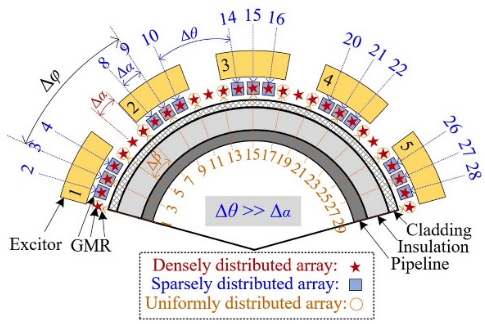

Figure 7. Comparison of the densely, sparsely and uniformly distributed GMR sensors array structures.

space between the last GMR element of the front group and the first GMR element of the latter group is $\Delta\theta$, then the following relationship should exist: $\Delta\theta \gg \Delta\alpha$. Note that the common 15 GMR sensors of the sparsely and densely distributed CAA array are located right under the five peaks with respect to the 5 excitors; while the other 14 GMR sensors in the densely distributed array appear at the sunken area of the magnetic field. In practice, although the use of 14 GMR sensors located in the sunken area may offer higher resolution, it is not cost-effective to cover the sunken area by considering the complexity of mechanical and electronic structures. For example, the installations of the 6th, 12th, 18th, 24th GMR sensor are quite inconvenient since they are located in the blank position of the detector mechanical structure. Moreover, without loss of generality, we should use the same number of receivers to further analyze the difference between the sparse and other kinds of arrays. Specifically, we compared the sparse CAA with a uniformly distributed structure, where the uniform CAA array consists of 15 GMR sensors with index of $\{1; 3; 5; 7; 9; 11; 13; 15; 17; 19; 21; 23; 25; 27; 29\}$ as shown in figure 7. It is obvious that the uniform array elements with interval of $\Delta\beta$ are located in both peak and sunken areas, and the signal strength of GMR sensors in sunken area will be too small to obtain enough SNR for corrosion inspection.

Table 2. Parameters of the simulation and experiment.

Parameter	Value
Width of each excitor	25 mm
Length of each excitor	30 mm
Height of each excitor	25 mm
Number of the excitors	5
Interelement angle of excitors	20°
Number of turns for each excitor	600
Number of the GMR sensors	15
Interelement angle $\Delta\beta$ of the GMR sensors in the uniform CAA	6.2°
Angle $\Delta\alpha$ of the GMR sensors in the sparse CAA	3.1°
Angle $\Delta\theta$ of the GMR sensors in the sparse CAA	12.4°
Outer diameter of the pipelines	152.4 mm
Thickness of the insulation layer	60 mm

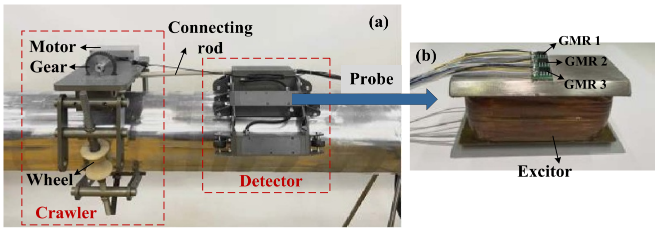

Figure 8. Assembled sparse CAA-based PEC inspection system. (a) Automatic pipeline-inspection system. (b) Probe structure.

5. Experimental results

The validity of the proposed CAA-based PEC inspection system for thermally insulated pipelines was confirmed by experiments, and the parameters of which are the same as those employed for the simulations in the previous sections, as listed in table 2.

Figure 8 shows the assembled CAA-based PEC system for the CUI inspection of the pipelines, corresponding to the information in figure 3. The system comprises an automatic pipeline-inspection crawler and a detector. As shown in figure 8(a), a standard 6-inch pipeline was inspected, which was wrapped with a 60-mm insulation layer (rock wool), and a layer of thin aluminum plate (0.5 mm) was wrapped outside the insulation layer. Figure 8(b) shows one of the five probes described in our simulation and experiments, comprising one excitor and three GMR sensors with dimensions of 30 mm × 25 mm × 25 mm and 6.2 mm × 5 mm × 1.3 mm, respectively. Note that each of the five excitors in figure 8(a) was excited at a current of 1 A.

In our experiments, six corrosion defects with respect to three types (holes, rings, and cracks) in the standard six-inch pipeline were inspected to verify the performance of the proposed CAA-based PEC inspection system for thermally insulated pipelines. Figure 9 shows six corrosion defects, termed Hole-1, Hole-2, Ring-1, Ring-2, Crack-H, and Crack-V, respectively, where the centers of the defects are all in the middle of each pipeline.

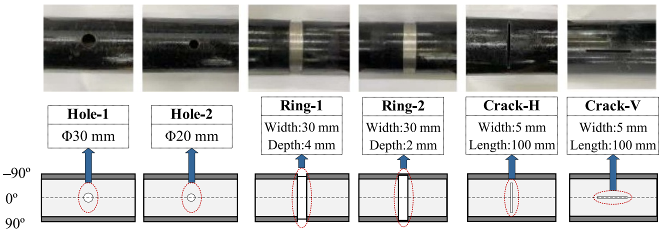

Figure 9. Diagram of the measured pipelines with corrosion defects from $-90°$ to $90°$.

Considering the Hole-1, Hole-2 defects and the position without defect as examples, figure 10 shows the experimental results of a single excitor and multiple excitors (uniform and sparse CAAs) for all sampling times. In figure 10, the middle of the hole defects in circumferential direction are assumed to be aligned with the 8th GMR sensor that is in the middle of the CAA, which is considered as the ideal case. For the single excitor case in figure 10(a), only the middle (the third of the CAA) excitor was excited with a current of 1 A, and the responses of the 8th GMR sensor for the single and multiple excitor cases are compared.

As shown in figure 10(a), the response curves with single excitor and multiple excitors are similar for two type of hole defects, which demonstrated the effectiveness of multiple excitors for the inspection of CUI. Additionally, figures 10(b)–(d) compare the responses of all 15 GMR sensors of the sparse CAA for each case. As shown in figure 10(b), all 15 curves are much similar, which indicates no defects exist in the pipe, and the little differences between each GMR sensor are caused by the waviness effect due to the multiple excitors. As comparisons, the 15 curves in figures 10(c) and (d) appear great difference corresponding to the several GMR sensors nearby the 8th one of the sparse CAA, while the others stay almost the same as the figure 10(b). Obviously, the differences between different GMR sensors in figures 10(c) and (d) is mainly caused by the hole defects, which facilitate the inspection of the defects, because the outputs of the GMR sensors near the holes in figures 10(c) and (d) changed more noticeably as compared with the case of the pipeline without defects shown in figure 10(b). As a result, it can be indicated that the hole defect exists around the 8th (middle) GMR sensor, and figure 10(c) has a larger defect than figure 10(d). Using this property, the CUI inspection can be realized more efficiently by using the CAA structure with larger coverage area of magnetic field. Notably, by choosing proper sampling times, it is possible to improve the performance of the CAA-based PEC inspection system for thermally insulated pipelines. The optimization of the sampling times will be addressed in our future work. As a comparison shown in figures 10(e) and (f), the 15 curves of 15 GMR sensors of the uniform CAA corresponding to Hole-1 and Hole-2 are much different from the sparse CAA, where the waviness effect plays more important role to have influence on the GMR sensor outputs. Specifically, the GMR sensors (1st, 3rd, 4th, 6th, 7th, 9th, 10th, 12th, 13th, 15th of the uniform array) located at the sunken area show lower output values than the GMR sensors with the same index in the sparse array

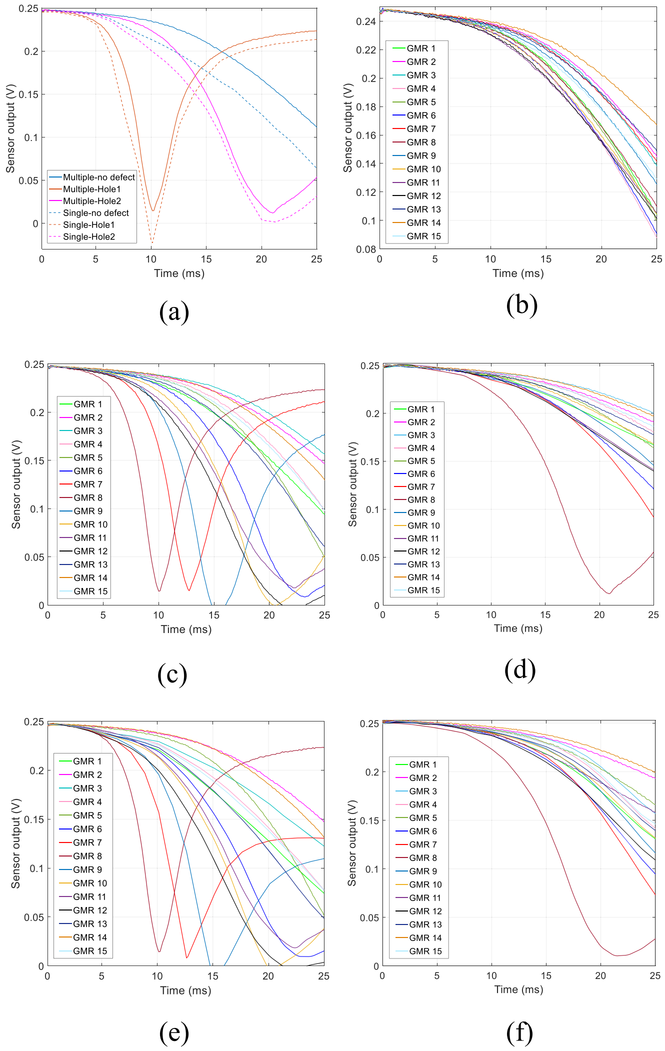

Figure 10. Experimental results of the sparse and uniform CAAs. (a) The 8th GMR sensor output for the single and multiple excitor cases for different pipeline defects. (b) The output of the sparse CAA for the pipeline without defects. (c) The output of the sparse CAA for Hole-1. (d) The output of the sparse CAA for Hole-2. (e) The output of the uniform CAA for Hole-1. (f) The output of the uniform CAA for Hole-2.

as shown in figures 10(c) and (d), which will make the inspection of the defects more complicated.

To further investigate the inspection performance of the sparse CAA, we took the data with sampling time of 10 ms as examples, and figures 11 and 12 compare the imaging results of the original outputs of the PEC inspection system using uniform and sparse CAAs described in section 4 for the experimental pipeline structure, respectively.

Similar to figure 10, in figures 11 and 12, the middle of the hole and crack defects in circumferential direction are aligned with the 8th GMR sensor that is in the middle of the CAA. We can observe that there exist six types of 'nulls' that correspond to the six corrosion defects in figure 9. And the main differences between uniform and sparse CAAs in the imaging results for all types of corrosion defects are the SNR of the image in part of the GMR sensor channels that correspond to

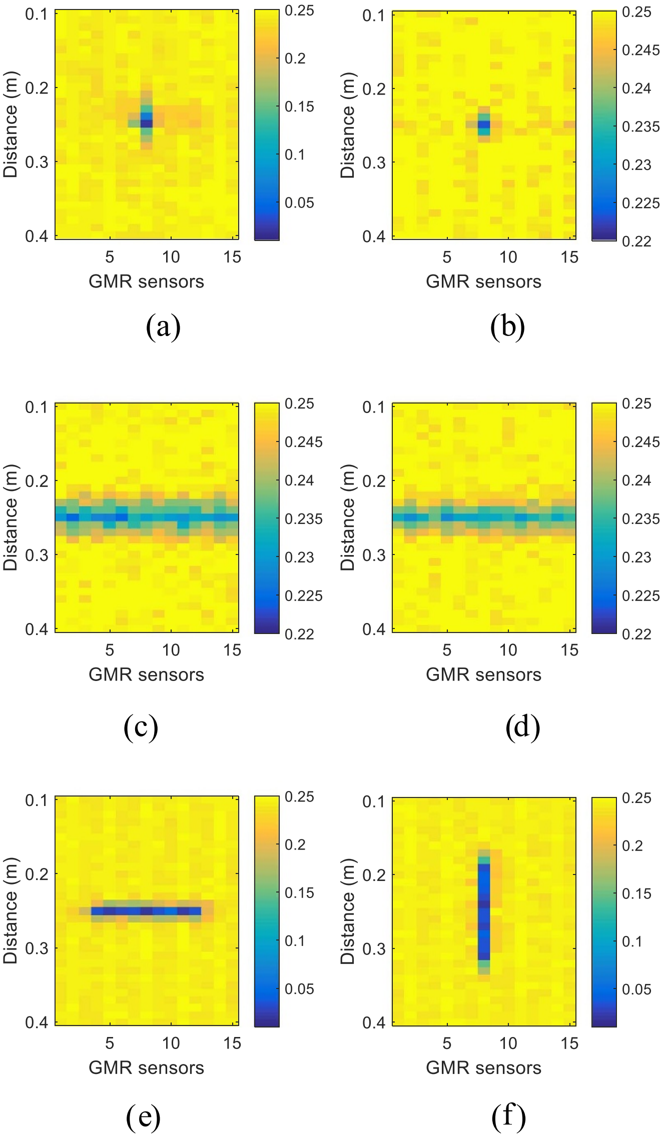

Figure 11. Inspection results of the uniform CAA for different corrosion defects. (a) Inspection result for Hole-1. (b) Inspection result for Hole-2. (c) Inspection result for Ring-1. (d) Inspection result for Ring-2. (e) Inspection result for Crack-H. (f) Inspection result for Crack-V.

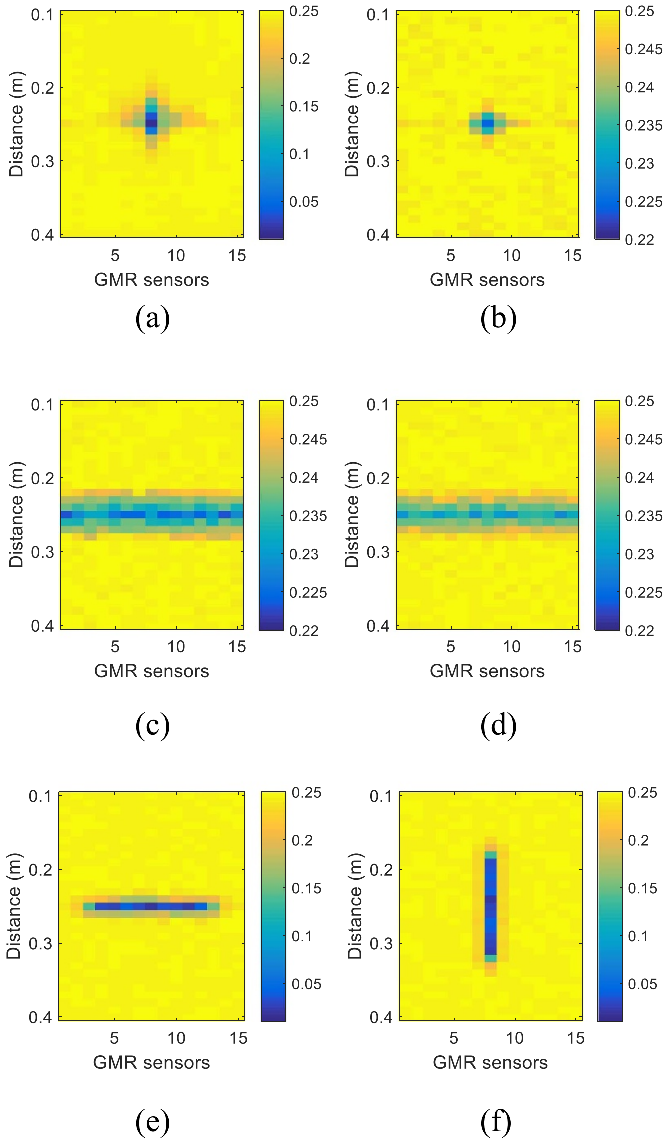

Figure 12. Inspection results of the sparse CAA for different corrosion defects. (a) Inspection result for Hole-1. (b) Inspection result for Hole-2. (c) Inspection result for Ring-1. (d) Inspection result for Ring-2. (e) Inspection result for Crack-H. (f) Inspection result for Crack-V.

the sunken area. Specifically, the imaging shapes of the sparse CAA for asymmetry corrosion defects are more regular and easier to be identified than those of the uniform CAA. This is mainly because of the increase of the signal strength. Notably, although the sparse CAA can effectively identify the pipeline defects under the insulation layer, the inspected shapes in figure 12 are greater than the actual shapes because of the existence of a large lift-off distance from the thermal insulation layer.

Without loss of generality, since the GMR sensor may not always be the ideal case that align with the middle of the corrosion defects in practice, by still considering the two hole-type defects as examples, we compared the inspection results of uniform and sparse CAAs for the worst-case scenario, where the defect center is located in the middle of the two GMR sensors (taking the hole defects at the middle of GMRs 6 and 7 as examples). The imaging results of the uniform and sparse CAAs are compared in figure 13.

Compared with figures 11 and 12, the positions of the hole defects in the imaging results of figure 13 derivate from the center to left due to the displacement of the hole center. Although the imaging results suffer a significant performance decrease and appear to be changed in the defect shapes, the outputs of the sparse CAA in figures 13(c) and (d) are more clear to identify the corrosion defects than that of the uniform CAA in figures 13(a) and (b) due to the improvement of SNR in part of the GMR sensor channels that correspond to the sunken area. Specifically, the SNR can be improved because of the increased signal strength benefitted by the sparsely distributed structure, so that the influence of the waviness effects

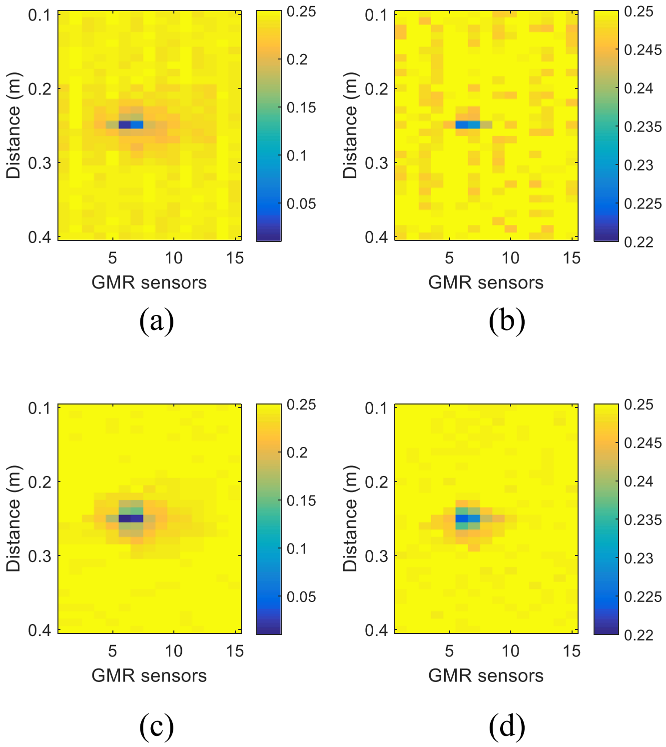

Figure 13. Inspection results for the hole defects in the worst-case scenario. (a) Inspection result of the uniform CAA for Hole-1. (b) Inspection results of the uniform CAA for Hole-2. (c) Inspection result of the sparse CAA for Hole-1. (d) Inspection results of the sparse CAA for Hole-2.

on the shape distortion due to the multiple excitors can still be well reduced. Notably, since the thickness of insulation layer (60 mm) is much larger than the inter-element distance of the GMR sensors array (about 7 mm), the differences of distances between the defect center to the neighbor GMR sensors become very small. As a result, the relative position of GMR sensors and excitors with respect to the peaks and sunkens will play a much more important role than that of the GMR sensors and defects. Furthermore, even though more GMR sensors may offer more information, it is not cost-effective to cover the sunken area due to the complexity of mechanical and electronic structures. For example, the installation of the 6th, 12th, 18th, 24th GMR sensor is quite inconvenient since they are located in the blank position of the detector mechanical structure. In the case of the same number of receivers are used for the CAA-based multiple excitors structure, the sparse CAA can offer higher SNR, and the resolution will not be significantly affected as compared to the uniform CAA structure.

6. Conclusion

In this study, a sparse CAA-based PEC inspection system for thermally insulated pipeline to improve the measurement efficiency was designed. Based on the PEC model, multiple excitors were employed to synthesize magnetic fields in a large range around the pipelines, and an automatic pipeline-inspection crawler, as well as the corresponding circuits, were also developed. Moreover, we designed a sparsely distributed receiver CAA structure to eliminate the waviness distribution of the eddy current fields due to the multiple excitors, where the SNR of the CAA-based PEC inspection system can be significantly improved. Simulations and experiments on standardized oil-well casings with several defects demonstrated the effectiveness of the proposed system.

Data availability statement

All data that support the findings of this study are included within the article (and any supplementary files).

Acknowledgments

The authors would like to thank the reviewers for their helpful suggestions, which have considerably improved the quality of the manuscript.

Funding

This work was supported in part by the National Natural Science Foundation of China under Grant 51974250, in part by the Youth Science and Technology Nova Project in Shaanxi Province, China, under Grant 2020KJXX-018 and in part by the Youth Scientific Research and Innovation Team Construction Plan Project of Xi'an Shiyou University under Grant of 2022QNKYCXTD02.

ORCID iDs

Ling Yang https://orcid.org/0000-0001-9794-9324
Jingxin Dang https://orcid.org/0000-0001-6213-1565
Yan Zhou https://orcid.org/0000-0002-5534-7955
Bo Dang https://orcid.org/0000-0002-9258-0764

References

[1] Abubakirov R, Yang M and Khakzad N 2020 A risk-based approach to determination of optimal inspection intervals for buried oil pipelines *Process. Saf. Environ. Prot.* **134** 95–107
[2] Cao Q, Pojtanabuntoeng T, Esmaily M, Thomas S, Brameld M, Amer A and Birbilis N 2022 A review of corrosion under insulation: a critical issue in the oil and gas industry *Metals* **12** 561
[3] Marquez A, Singh J and Maharaj C 2021 Corrosion under insulation examination to prevent failures in equipment at a petrochemical plant *J. Fail. Anal. Prev.* **21** 723–32
[4] Wiggen F, Justnes M and Espeland S 2021 Risk based management of corrosion under insulation *SPE Int. Oilfield Corrosion Conf. and Exhibition*
[5] NACE Standard 2017 SP0198; Control of corrosion under thermal insulation and fire proofing materials—a systems approach (NACE)
[6] Hernandez J, Fouliard Q, Vo K and Raghavan S 2022 Detection of corrosion under insulation on aerospace structures via pulsed eddy current thermography *Aerosp. Sci. Technol.* **121** 107317

[7] Jacques R C, Oliveira H, Santos R and Clarke T G R 2019 Design and in situ validation of a guided wave system for corrosion monitoring in coated buried steel pipes *J. Nondestruct. Eval.* **38** 1–12

[8] Cho H, Tamura Y and Matsuo T 2011 Monitoring of corrosion under insulations by acoustic emission and humidity measurement *J. Nondestruct. Eval.* **30** 59–63

[9] Jones R E, Simonetti F, Lowe M and Bradley I P 2012 Use of microwaves for the detection of water as a cause of corrosion under insulation *J. Nondestruct. Eval.* **31** 65–76

[10] Chizh M, Zhuravlev A, Razevig V, Ivashov S, Falorni P and Capineri L 2020 Defects investigation in thermal insulation coatings with microwave imaging based on a 22 GHz holographic radar *NDT&E Int.* **109** 29–36

[11] Franke D 2022 Corrosion under insulation—prevention, control and detection *Int. Sugar J.* **124** 108–15

[12] Safizadeh M S, Liu Z and Lepine B A 2004 Multifrequency eddy current for the characterization of corrosion in multilayer structures *Mater. Eval.* **62** 535–9

[13] Chen X and Niu H 2022 Pulsed eddy current testing for gap measurement of metal casing *Meas. Sci. Technol.* **33** 075108

[14] Yu Z, Yang F, Fu Y and Huang W 2021 Investigation of focusing properties of probes for pulsed eddy current testing *IEEE Sens. J.* **21** 26830–8

[15] Song Y and Wu X 2022 An analytical solution for vertical coils near a multi-layered metallic pipe in pulsed eddy current testing *NDT&E Int.* **125** 102570

[16] Wang H, Huang J, Liu L, Qin S and Fu Z 2022 A novel pulsed eddy current criterion for non-ferromagnetic metal thickness quantifications under large liftoff *Sensors* **22** 614

[17] Li Z *et al* 2020 Simulation analysis of three-dimensional finite element model about the corrosion defect of pipeline *2019 14th IEEE Int. Conf. on Electronic Measurement & Instruments (ICEMI)* (IEEE)

[18] Nafiah F, Tokhi M O, Shirkoohi G, Duan F, Zhao Z and Rees-Lloyd O 2021 Decoupling the influence of wall thinning and cladding thickness variations in pulsed eddy current using principal component analysis *IEEE Sens. J.* **99** 22011–8

[19] Long Y, Huang S, Zheng Y, Wang S and Zhao W 2020 A method using magnetic eddy current testing for distinguishing ID and OD defects of pipelines under saturation magnetization *Appl. Comput. Electromagn. Soc. J.* **35** 1089–98

[20] Angani C S, Park D G, Kim C G, Leela P, Kollu P and Cheong Y M 2010 The pulsed eddy current differential probe to detect a thickness variation in an insulated stainless steel *J. Nondestruct. Eval.* **29** 248–52

[21] Park D G, Kishore M B, Kim J Y, Jacobs L J and Lee D H 2016 Detection of corrosion and wall thinning in carbon steel pipe covered with insulation using pulsed eddy current *J. Magn.* **21** 57–60

[22] Cheng W 2012 Pulsed eddy current testing of carbon steel pipes' wall-thinning through insulation and cladding *J. Nondestruct. Eval.* **31** 215–24

[23] Xiao X T, Liang Z, Tang S and Zhang L 2021 Design and experiment of a two-coil magnetic core inductor used for the stepped eddy current thermography technique *IEEE Sens. J.* **21** 27549–60

[24] Fan X, He Y, Chen T and Hou C 2022 Research on crack monitoring technology of flexible eddy current array sensor based on TMR sensors *Measurement* **192** 110926

[25] Sirois M, Bouchard M and Sweedy A 2020 Advanced eddy current array tools for stress corrosion cracking direct assessment on pipelines *2020 13th Int. Pipeline Conf.*

[26] Zhang N, Ye C, Peng L and Tao Y 2021 Eddy current probe with three-phase excitation and integrated array TMR sensors *IEEE Trans. Ind. Electron.* **68** 5325–36

[27] Mizukami K, Hioki S, Moriyama K, Ogi K, Miyaji W and Kimura K 2021 Eddy-current array-probe technique for imaging near-surface and deep-lying delaminations in multidirectional carbon fiber composites *Compos. Struct.* **276** 114537

[28] Yang L, Wang X, Sun T, Meng T, Yang X, Li L and Qi Y 2022 A technology of full perimeter inspection for steel pipeline without removing cladding *Measurement* **190** 110746

[29] Joseph B, Long N and Arvid H 2017 Eddy current testing with giant magnetoresistance (GMR) sensors and a pipe-encircling excitation for evaluation of corrosion under insulation *Sensors* **17** 2229

[30] NVE 2014 GMR magnetic sensors application notes (available at: www.nve.com/SensorApps.php)